Multi-chirp LFM Waveforms Generation with Reconfigurable Chirp Rates Using Optical Injection in a Semiconductor Laser

B. Nakarmi, *Senior Member, IEEE,* Y.S. Bai, I. A. Ukaegbu, *Senior Member, IEEE,* H. N. Parajuli, *Member, IEEE,* A. Ashimbayeva, *Student Member, IEEE,* U. Nakarmi, *Member, IEEE,* X. Wang, and S. Pan, *Fellow, IEEE*

***Abstract*—We propose and experimentally demonstrate a photonics-based technique for generating simultaneous up-down multiple chirp-rate linear frequency modulated (SUDMC-LFM) waveforms using a dual beam injection technique in a distributed feedback (DFB) laser. To generate waveforms with multiple chirps, drive waveforms of different amplitude-time slopes for each sub-interval time are designed in an arbitrary waveform generator (AWG) and fed into the intensity modulator, which in turn, controls the intensity of the injected beam. Consequently, the rate of redshift of the emission wavelength is controlled. In the experiment, the intensity of only one beam is controlled with the designed AWG signal. For the proof-of-concept demonstration, we generate continuous multiple chirps (CMC), simultaneous up-down multiple chirps (SUDMC), and simultaneous up-down frequency hopped multiple chirps (SUDFHMC) LFM waveforms. Furthermore, re-configurability of the generated waveforms in terms of center frequency, bandwidth, number of chirps and chirp-rates are obtained by either changing the wavelength of the injected beams or by changing the parameters of the AWG signal. In the experiment, the SUDFHMC waveform with four frequency-hopping with sub-interval chirps of 4 GHz/µs, 1.2 GHz/µs, 2.4 GHz/µs, and 2.8 GHz/µs for both the up-chirps and down-chirps, respectively is generated. The auto-ambiguity analysis at -3 dB full-width half maximum (FWHM) shows the time-bandwidth product (TBWP) of >4545, and unambiguous Doppler of <0.75 MHz for CMC, SUDMC, and SUDFHMC signals with three chirps. These results indicate that the proposed waveforms have the potential to provide high performance in multi-radar and multi-target applications.**

***Index Terms*— Linear frequency modulation, multiple chirps, dual LFM, microwave photonics, optical injection, radar**

I. Introduction

Today's practical radio detection and ranging (radar) systems are mostly based on electronics and therefore suffer from the limited bandwidth of electronic devices; the increase in noise level with increasing center frequency and bandwidth; and the limited tunability of design parameters of the radar systems. To overcome these limitations, several approaches based on microwave photonics (MWP) have been reported. Photonics offers several advantages which include the generation, detection, and processing of high-bandwidth and high-frequency signals, ranging from microwaves (MW) to millimeter waves (mm-waves) [1-6]. One of the earliest demonstrations of an MWP-based radar system uses coherent beating of mode-locked laser (MLL) wavelengths [7]. The bandwidth of such a system depends on the repetition rate of the MLL, and therefore, a lower repetition rate resulting to poor range resolution. Subsequently, photonics-based frequency multiplication techniques have been demonstrated using advanced electro-optic modulators with improved resolutions [8, 9]. These methods are worth noting because of the simple operation, as only one modulator is used. Nevertheless, the frequency and bandwidth of the generated signal depend on the radio frequency (RF) source and require a high-frequency source. Also, there have been few research works using optical injection in a semiconductor laser to generate radar signals [10-14]. The optical injection technique does not require a high-frequency RF signal sousrce or a complex configuration but can be extended to generate different types of waveforms [10, 11].

Among different waveforms used in radar systems, linear frequency modulated (LFM) waveform with a single chirp, either up-chirp or down-chirp [2, 4-6, 8-14] is most commonly used. In a single chirp LFM signal, the range-Doppler resolution significantly degrades [15]. This degradation can be improved by using complementary dual chirp signals [14-16], or by using band fusion of narrowband signals [17, 18]. Additionally, the use of single chirp LFM signal without advanced signal processing is ineffective in mitigating interference and spoofing in radar detection, and is not well-suited for modern day's complex multi-radar and multi-target

Manuscript received xx, xxxx. This work was supported in part by Nanjing University of Aeronautics and Astronautics (90YAH21066), Nazarbayev University Collaborative Research Grant (11022021CRP1507), and the Ministry of Education and Science of the Republic of Kazakhstan (AP14871109).

B. Nakarmi, Y. S. Bai, X. C. Wang and S. L. Pan are with the Key Laboratory of Radar Imaging and Microwave Photonics (Nanjing Univ. Aeronaut. Astronaut.), Ministry of Education, Nanjing University of Aeronautics and Astronautics, Nanjing 210016, China (e-mail: bikash@nuaa.edu.cn; e-mail: pans@ieee.org).

U. Nakarmi is with the Department of Computer Science and Computer Engineering at the University of Arkansas, AR, USA.

I.A. Ukeagbu, H. N. Parajuli and A. Ashimbayeva are with the Integrated Device Solutions and Nanophotonics (iDSN) Laboratory, Electrical Engineering Department, School of Engineering and Digital Sciences, Nazarbayev University, 010000 Astana, Kazakhstan.

situations [19-21]. A few solutions in the electronic domain for mitigating interference include the use of anti-interference waveforms [22-24], adaptive noise cancellation in the receiver [25], and an electronic hardware-based approach [26]. However, due to the bandwidth limitations of electronic devices, photonic approaches are required for high-bandwidth radar systems. A limited number of photonics-based approaches have been previously demonstrated to address interference issues for high bandwidth radar signals [27, 28], but these demonstrations are limited to single chirp-rate waveforms.

Hence, in this paper, we propose and experimentally demonstrate a new type of robust waveform, namely, simultaneous up-down multiple chirp-rate LFM (SUDMC-LFM) using the dual beam injection technique in a distributed feedback (DFB) semiconductor laser. The injection of an external master laser (ML) beam into the DFB slave laser (SL) causes a change in the refractive index, which leads to a redshift of the emission wavelength of the DFB laser [29, 30]. The basic principle of the almost linear redshift phenomenon is modified for controlled redshift by applying a predesigned arbitrary waveform generator (AWG) signal. Among different dynamical states that can be invoked with a semiconductor laser, in the proposed scheme, Period one (P1) oscillation in a DFB laser is achieved with two beam injections, where only the intensity of one beam is controlled by different amplitude-time slope signals generated through the AWG, thus, resulting in a different rate of redshift of the emission wavelength of the DFB laser. The power of ML is set in such a way that the SL does not go into strong injection locking, thus preventing the suppression of the SL and ensuring sufficient power of the RF signal at the output. On optical beating between the redshifted emission mode with different redshift rates and the injected dual beams, simultaneous up-down multiple chirp rate LFM can be generated. In this manuscript, three types of robust LFM waveforms are generated: a) continuous multiple chirps (CMC), b) simultaneous up-down multiple chirps (SUDMC), and c) simultaneous up-down frequency-hopped multiple chirps (SUDFHMC). As a verification of the proposed scheme, we demonstrated a CMC waveform with a total bandwidth of 7.5 GHz (8 GHz – 15.5 GHz) with three chirp-rates of 7.5 GHz/µs, 12 GHz/µs and 3 GHz/µs within a total time period of 1µs. Similarly, SUDMC with 3 GHz/µs, 4 GHz/µs and 3.6 GHz/µs chirp rates for both up-chirp (8 GHz – 11.5 GHz) and down-chirp (15 GHz - 11.5 GHz) is demonstrated. Furthermore, the SUDFHMC waveform with four LFM frequency hopping steps and with the individual chirp-rates of 4 GHz/µs, 1.2 GHz/µs, 2.4 GHz/µs and 2.8 GHz/µs for up-chirp (11 GHZ - 13.6 GHz) and down chirp (18.5 GHz – 15.9 GHz) is demonstrated. It is apparent that with the above results, the same configuration can be used to generate several types of radar waveforms with reconfigurable parameters such as frequency, bandwidth, number of chirps, chirp-rate and hopping steps.

Moreover, the auto-ambiguity function analysis is performed to evaluate the range-Doppler resolution of the three aforementioned cases for an identical time interval of 1 µs and a bandwidth of 7 GHz. From the analysis, the -3 dB FWHM delay and Doppler for CMC with three chirps are found to be 0.22 ns and 0.72 MHz, respectively. Furthermore, a -3 dB FWHM delay of 0.16 ns and a Doppler of 0.72 MHz are obtained for the SUDMC with three chirps, while a -3 dB FWHM delay of 0.18 ns and a Doppler of 0.75 MHz are obtained for the SUDFHMC with three chirps.

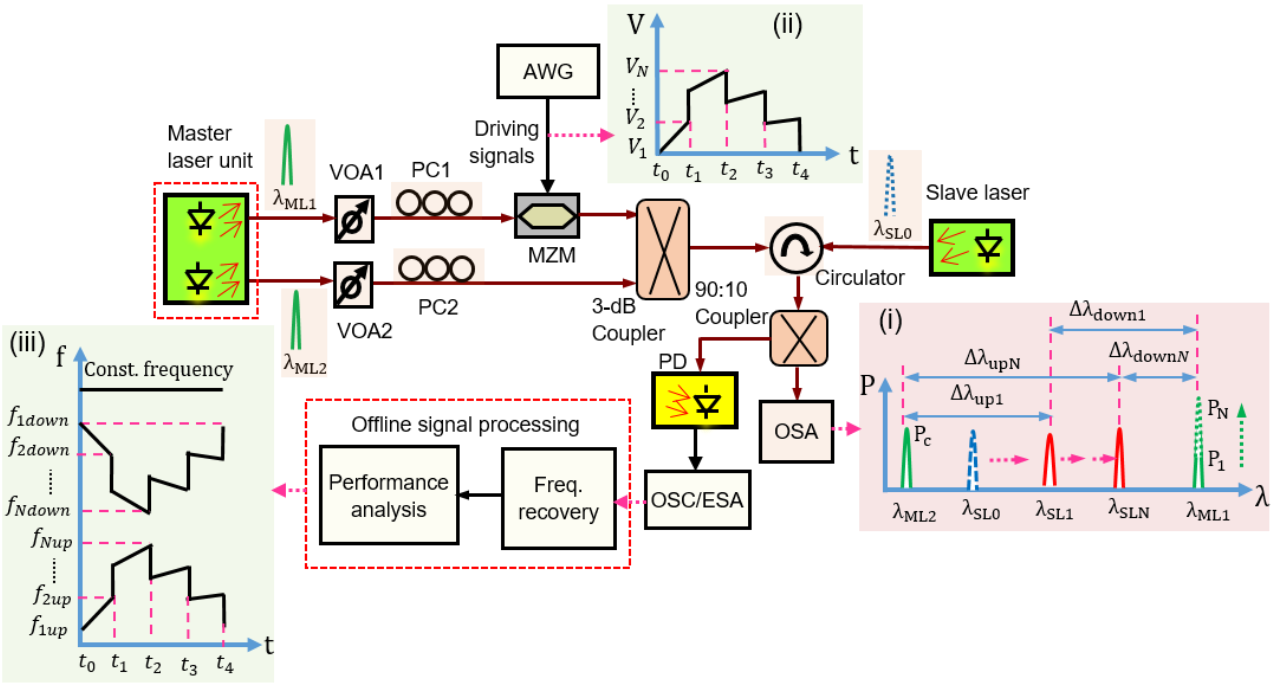

Fig. 1 Functional block diagram of the experimental setup. Insets; (i) the generated optical spectra with two beams injections, (ii) the driving signal with varying voltage-time slopes between each sub-intervals, and (iii) generated frequency-time waveform after O/E conversion.

II. Experimental Setup

The experimental block diagram of the proposed SUDMC-LFM waveform generation method is shown in Fig. 1. The experimental setup comprises a tunable laser (Agilent N7714A) which is used as a master laser (ML), can emit light of wavelengths in the range from 1535 nm to 1565 nm and power in the range from 8 dBm to 16 dBm. Two output ports of this laser unit are used as two master lasers, namely ML1 and ML2 for the generation of SUDMC and SUDFHMC signals, while single output (ML1) is used for CMC generation. The polarization-dependent C-band DFB laser (Actech LD15DM) is used as an SL and is biased with a 30 mA driving current using the low noise (0.2 μA) Thorlabs LDC205C laser driver. The temperature in the DFB mount is maintained at 25 ºC with the temperature controller (Thorlabs TED200C) so that it is ensured that the DFB emits with a constant wavelength. Under these operating parameters, the DFB laser emits light at a wavelength of 1541.96 nm with a power of -10 dBm. For the CMC generation, ML1 is set to a wavelength of 1541.878 nm with an emission power of 10 dBm and injected into the SL. In the cases of SUDMC and SUDFHMC, ML1 and ML2 are operated at the wavelengths of 1542.12 nm and 1541.86 nm respectively. The SUDMC and SUDFHMC generation is a result of the combined effect of both ML1 and ML2. After maintaining the ML1 power at 10 dBm and ML2 power at 5 dBm through VOA1 and VOA2, respectively, for RF generation, the ML2 power is not further adjusted. Whereas, the output of ML1 is fed into a polarization-dependent 10 GHz Mach-Zehnder Modulator (MZM) (Lucent 2623NA) via a variable optical attenuator (VOA1) and polarization controller (PC1). By varying the power of ML1 through the VOA1, a redshift in the wavelength of the DFB laser emission can be observed due to the change in the refractive index. The total shift of the redshift determines the bandwidth of the generated signal. The MZM has a half wave voltage (V_π) of 5V. Due to the phase stability, linearity, and flexibility in the reconfiguration of radar waveform parameters, external modulation with MZM has been used instead of direct modulation of the laser for the purpose of ML injection. The MZM is driven by a driving signal generated by the AWG (Agilent 85110A, 120 MHz). The desired driving signals with different amplitude-time slopes for CMC, SUDMC, and SUDFHMC are designed and loaded into AWG. Based upon the designed AWG signal, the intensity of the injected beam is varied, which is consequently used to control the redshift in the DFB laser. The polarization controllers, PC1 and PC2, are used to optimize the output of the MZM and to ensure that only TE-polarized light is coupled into the SL. The circulator is used to couple the injected beams into the DFB laser and to obtain the controlled redshifted output signal from SL based on the AWG driving signal. The 10% of the output signal (from the 90:10 coupler) is used to analyze the signal through a 0.02 nm resolution optical spectrum analyzer (Yokogawa AQ6370C), and 90% of the output signal is applied to the high-speed 40 GHz bandwidth photo-detector (PD) (u2t XPDV2120RA) for optical-to-electrical (O/E) conversion. The MW signal generated through the optical beating in PD is analyzed using an electronic oscilloscope (OSC), Keysight DSO-X92504A, and an electrical spectrum analyzer (ESA), Agilent E447A. The data recorded by these instruments are used for further offline signal processing. Since the generated signals have different center frequencies, the signal received from OSC is down-converted to baseband in frequency recovery unit using Hilbert transform and center frequency multiplication stages generated offline. Subsequently, the obtained signals are low-pass filtered and used to evaluate the performance of generated waveforms by calculating the auto-ambiguity functions.

III. Principles of Operation

When an external beam is injected into an SL, a P1 oscillation state is reached due to the nonlinear dynamics of the DFB laser, which causes the red shift of the emission wavelength in the DFB laser [29, 30]. The P1 oscillation occurs with a period whose reciprocal is equivalent to the difference in frequencies between the injected ML and the redshifted SL. For SUDMC and SUDFHMC generation, two injected beams, ML1 and ML2, are used, while for CMC only a single beam ML1 is used.

Assume that the injected wavelengths of ML1 and ML2 are λ_{ML1}, and λ_{ML2}, and that of SL is λ_{SL0}. After injecting ML1 with the power P_1, the redshift occurs in SL and the wavelength of SL shifts to λ_{SL1}. Inset (i) of Fig. 1 illustrates the effect of the injection of MLs into an SL. Depending upon the injection of the MLs whether with the positive or negative wavelengths detuning with the SL, three frequency components corresponding to the wavelength spacing of $\Delta\lambda_{up1} = |\lambda_{SL1} - \lambda_{ML2}|$, $\Delta\lambda_{down1} = |\lambda_{ML1} - \lambda_{SL1}|$ and $\Delta\lambda_{const1} = |\lambda_{ML1} - \lambda_{ML2}|$ respectively can be obtained after the O/E conversion. Since the generated frequency component corresponding to $\Delta\lambda_{const1}$ is not due to the beating of the wavelengths of ML with SL, this component remains constant even after varying the power of ML1. Thus, two different MW signals corresponding to $\Delta\lambda_{up1}$ for up-chirp, and $\Delta\lambda_{down1}$ for down-chirp can be generated simultaneously. To generate the MW signal with a certain bandwidth, the power of ML1 is varied to obtain the redshift in the DFB laser. As can be seen in Fig. 1(inset i), by varying the injection power strengths of ML1 from P_1 to P_N, the SL emission wavelength shifts from λ_{SL1} to λ_{SLN}, and as a result, frequencies corresponding to $\Delta\lambda_{up1}$ to $\Delta\lambda_{upN}$, and $\Delta\lambda_{down1}$ to $\Delta\lambda_{downN}$ can be obtained. The wavelength spacing of the emission wavelength between λ_{ML2} and λ_{SL1} determines the starting frequency corresponding to $\Delta\lambda_{up1}$. The total redshift at SL, which corresponds to $\Delta\lambda_{BWup} = |\lambda_{SL0} - \lambda_{SLN}|$, determines the bandwidth of the generated up-chirp signal. Similarly, the emission wavelength spacing between λ_{ML1} and λ_{SL1} determines the starting frequency corresponding to $\Delta\lambda_{down1}$, and the bandwidth of the down-chirp signal will be identical to $\Delta\lambda_{BWup}$. It should be noted that the injected beam λ_{ML1} should be injected in such a way that the total redshift due to the change in the power of ML1 is smaller than the wavelength detuning between λ_{ML1} and λ_{SL1}. Otherwise, either there is no RF signal generation due to the zero-wavelength difference between the redshifted SL and ML1 or there is a reversal in the chirp slope due to the position of ML or SL, i.e., the negative wavelength detuning becomes positive wavelength detuning, as the redshifted

wavelength becomes larger than that of ML1. In a single beam case, based on the injected beam whether positive or negative wavelength detuning, a down-chirp signal or an up-chirp signal, can be obtained, respectively.

In this experiment, we injected the ML power into SL via the MZM. The output power of MZM can be controlled through the input-driving electrical signal [31]. Thus, the change in the injected power can be obtained using the MZM with a modulating signal from the AWG. We biased the MZM at the linear point of the MZM transfer function curve so that the optimum linearity is ensured. The desired signals are written in MATLAB and loaded in the AWG, thus, serving as the driving signal for the MZM as shown in Fig. 1(inset ii). Through intensity modulation, the AWG signal controls the input injection power of ML1. For the MW signal generation with the desired bandwidth and chirp-rate, the AWG drive signal is designed with different amplitude-time slopes for different sub-intervals, which result in a corresponding redshift of the DFB emission wavelength. As a result, the amplitude-time slopes of the driving signal map to the frequency-time slopes of the generated MW signal after O/E conversion, as shown in Fig. 1(inset iii). In inset (iii), f_{1up} and f_{1down} correspond to the redshift due to V_1 whereas f_{Nup} and f_{Ndown} is obtained due to the redshift amount by V_N amplitude of the AWG signal. Similarly, the intermediate frequency values correspond to the amplitudes of the AWG signal. The abrupt jump in the frequency is due to the abrupt amplitude change in the AWG signal rather than linear change while doing a transition from one sub-interval to another. Also, due to the presence of different amplitude-time slopes in each sub-interval, the rate of redshift of the emission wavelength of a DFB laser for each sub-interval will be different. Upon optical beating of the AWG-controlled redshifted modes and the injected beams wavelengths, multiple chirp-rate signals can be obtained.

A. Redshift phenomenon and MW generation process with single and dual beam injections

Fig. 2 illustrates the redshift phenomena and MW generation process with a single beam injection. Fig. 2(a) shows the optical spectra at the output of the circulator. The dotted spectrum shows the spectrum of SL before the injection of ML1, which is centered at 1541.96 nm. With the injection of ML1 with a wavelength of 1541.878 nm and a power of 11 dBm, red shift phenomenon occurs due to the change in the refractive index, hence, causing a shift in the emission wavelength of the SL.

The inset shows the redshift of the SL when the power of ML1 changes from 11 dBm to 16 dBm. While changing the power of the ML1, not only the redshift occurs but also some power suppression of the emission mode for the SL is observed as shown in Fig. 2(a). In Fig. 2(b), the generated MW frequencies are shown as a function of ML1 power for different wavelength detuning. Upon the injection of ML1 with the negative wavelength detuning of 0.08 nm and the injection power of 11 dBm, the emission wavelength of SL shifted from 1541.96 nm to 1542.00 nm providing MW up-chirp signal with the starting frequency of 15.39 GHz, i.e., corresponding to the optical beating between the shifted wavelength of the SL and the ML1. Similarly, by changing the detuning wavelengths from 0.08 nm to 0.07 nm and 0.06 nm, MW signals with different starting frequencies can be generated as shown in Fig. 2(b). Thus, by choosing the proper power of ML1, the amount of redshift can be varied, whereas by setting the wavelength detuning, the starting frequency of the MW signal can be reconfigured as required. Furthermore, the phase noise associated with the presented optical injection technique with a P1 oscillation is less than -105dBc/Hz@10 kHz, therefore, no significant degradation is observed in the generated RF signal [32].

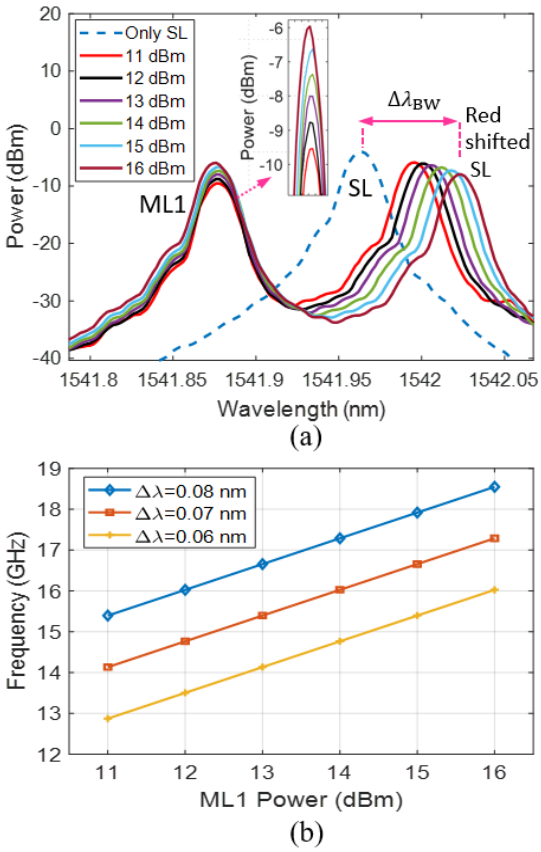

Fig. 2. Redshift and MW signal generation with one beam injection. (a) Optical spectrum. (b) Generated frequencies for different detuning and ML1 powers.

Fig. 3 illustrates the dual beam injection for generating simultaneous up- and down-chirp MW signal. It should be noted that in the dual beam configuration, rather than the total sum of redshift with the individual beam, the combined effect will be observed [14, 30]. In the experiment, two beams, ML1 and ML2, with wavelengths of 1542.12 nm and 1541.86 nm, are injected into the SL. Fig. 3(a) shows the optical spectra at the output of the circulator, for different injected powers. Fig. 3(b-i) provides details on the wavelengths, showing a redshift of 0.03 nm in SL when the power of ML1 varies from 10 dBm to 15.8 dBm, while the ML2 power is kept constant at 5 dBm. The beating of ML1 with the shifted SL generates a down-chirp signal with a starting frequency of 20.18 GHz, while the beating of ML2 with the shifted SL results in an up-chirp signal with a starting frequency of 12.61 GHz, as illustrated in Fig. 3(b-ii). Thus, as the power increment in ML1 causes a shift in SL wavelength, simultaneous up- and down-chirp signals can be generated. In this approach, the wavelength selection for ML1 and ML2 determines the starting frequencies and the total

amount of redshift determines the bandwidth of the generated MW signal.

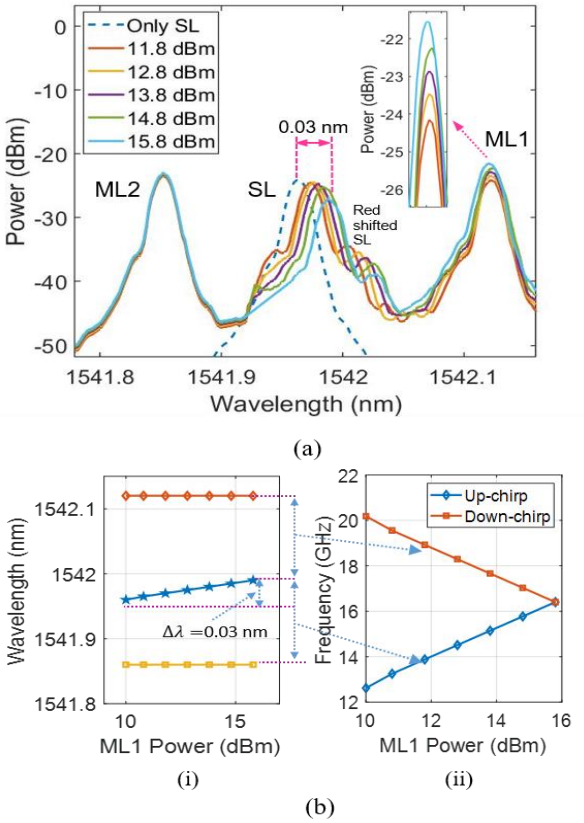

Fig. 3. Redshift and MW signal generation with two beam injections. (a) Optical spectrum at the output of the circulator. (b-i) Wavelengths shift, and (b-ii) simultaneous generation of up-chirp and down-chirp MW signals by beating different wavelengths.

In this experiment, we control the intensity of ML1 through a pre-designed AWG waveform. By controlling the amplitude-time slopes of the AWG-generated waveform, the rate of change in the injected intensity of ML1 into the SL with time can be controlled. This allows for the control of the redshift rate and thus chirp-rates of the generated MW signal, i.e., the amplitude-time slopes of the AWG waveform are mapped to the chirp rates of the generated waveform. Therefore, the amplitude-time slopes within the given time period of the driving signal determine the chirp rates of the generated RF signal, which will be verified in the following section IV with the experimental results. Thus, with the dual beam injection, simultaneous up-down multiple chirp-rate signal can be generated by designing the AWG waveform with multiple amplitude-time slopes within the given interval.

IV. Results and Discussion on the Generation of Multi-Chirped Waveforms

After analyzing the redshift of the emission wavelength of the SL, various types of AWG signals with different amplitude-time slopes within the given interval are designed to obtain different redshift rates. To demonstrate the control of the redshift rate and consequently the generation of multiple chirp rate signals, we experimentally demonstrated the generation of CMC, SUDMC and SUDFHMC waveforms. The CMC waveform consists of either up-chirp or down-chirp signal whereas SUDMC and SUDFHMC waveforms consist of simultaneous up-chirp and down-chirp signals.

A. CMC

The ML1 is injected into SL via the MZM. To generate the CMC signal with three chirps, a control signal with three different amplitude-time slopes is generated through the AWG, as shown in Fig. 4(a), and fed to the MZM. In the designed control signal, the 1 μs interval is divided into two 0.5 μs sub-intervals with voltage ranges of 0 V - 1.9 V and 1.9 V - 3.0 V, resulting in different amplitude-time slopes, leading to a different rate of redshift in the SL. Additionally, it is noted that the amplitude-time slope is not linear. The non-linear amplitude-time slope is used to compensate for the non-linear dynamics of the semiconductor laser that causes a non-linear redshift of the emission wavelength of the SL on a linear variation of the injected optical power. As different amplitude-time slopes are applied, different chirp-rate LFM signals are generated in each sub-interval after O/E conversion which is due to the change in the redshift rate with the applied AWG signal. The optical spectrum of the output of SL after applying the AWG signal to the MZM is shown in Fig. 4(b). The dotted line is a spectrum of SL before applying ML. With the implementation of the AWG signal, as shown in Fig. 4(a), multi-chirp signal with three sub-intervals and the chirp-rates

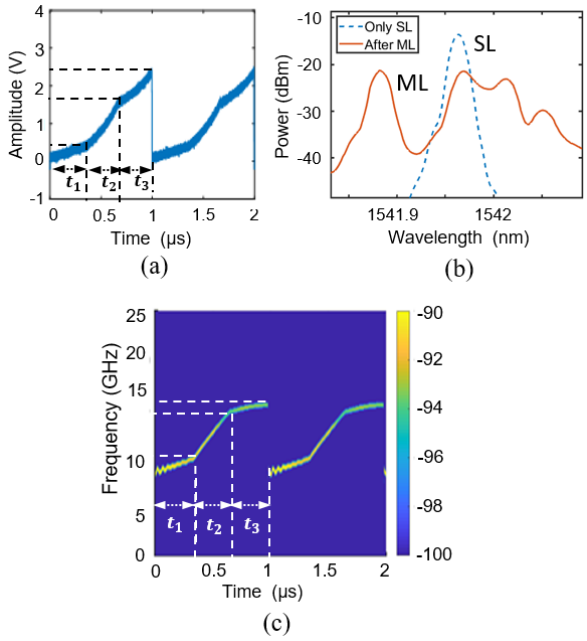

Fig. 4. CMC generation with three chirps. (a) Amplitude-time AWG signal, (b) optical spectrum of output of SL, and (c) frequency-time diagram of the generated signal.

of 7.5 GHz/μs (8.0 GHz - 10.5 GHz), 12 GHz/μs (10.5 GHz - 14.5 GHz), and 3 GHz/μs (14.5 GHz - 15.5 GHz), and a total bandwidth of 7.5 GHz (starting frequency of 8.0 GHz and an ending frequency of 15.5 GHz) is obtained, as shown in Fig. 4(c). The captured generated RF signal in the oscilloscope is

without employing an RF amplifier and noise reduction technique. In Fig. 4(c), a minor jitter is observed in the first chirp signal. This jitter may be due to the amplitude fluctuation in the driving signal which affects the amount of redshift in the emission wavelength of the DFB laser and consequently the frequency at the output. Hence, this jitter can be further reduced and removed by stabilizing the amplitude fluctuation and using a more stable AWG-generated control signal. Furthermore, by designing the AWG signal with multiple amplitude-time slopes in a given interval, the CMC signal with reconfigurable chirp rates, starting frequencies, bandwidths, and number of chirps can be obtained which is discussed further in the following section B.

B. SUDMC and SUDFHMC

In this case, two ML beams, ML1 and Ml2, are injected into the SL, among which only ML1 is coupled via MZM. The

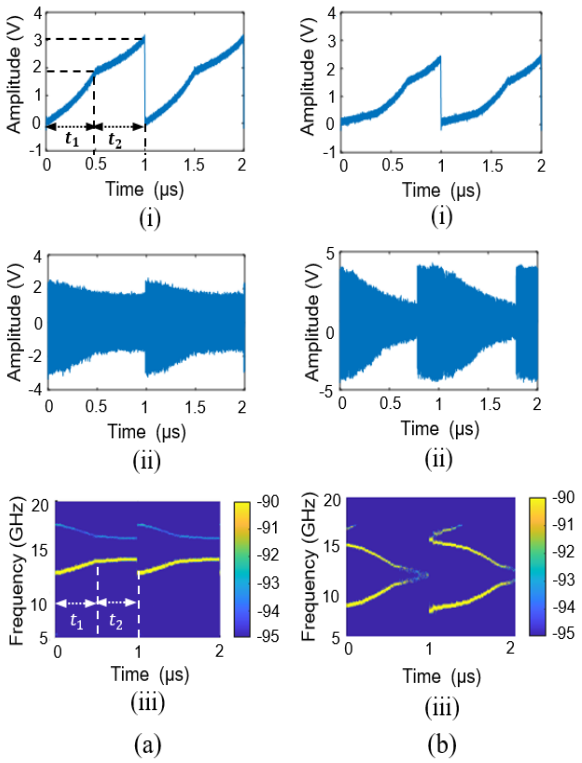

Fig. 5. SUDMC generation with (a) two chirps and (b) three chirps. (i) Amplitude-time AWG signal, (ii) instantaneous waveform of the generated signal, (iii) frequency-time diagram of the generated signal.

injected power and wavelength of ML1 are controlled similarly as in the CMC case, while ML2 is kept constant as shown in Fig. 1. To generate the SUDMC waveform with two chirp-rates at each up/down-chirp, an amplitude-time control signal with two different slopes in the interval of 1 μs is designed and generated by AWG, as shown in Fig. 5(a-i). The 1-μs interval is divided into two 0.5-μs subintervals with voltage ranges of 0 V - 1.9 V and 1.9 V - 3.0 V, so that the two sub-intervals have different amplitude-time slopes, causing a different rate of redshift in the SL. As in the CMC, the starting frequency is determined by wavelength detuning of ML1 and Ml2 with the emission mode of SL, and the chirp-rate in each interval is determined by the amplitude-time slope of the AWG signal for the respective sub-interval. Fig. 5(a-ii) shows the captured amplitude-time RF signal from the oscilloscope after O/E conversion which is the result of applying amplitude-time driving signal as shown in Fig. 5(a-i). The AWG signal has dissimilar amplitude ranges (dissimilar slopes) for each sub-interval, as depicted in Fig. 5(a-i). The change in the amplitude -time signal not only provides redshift but also slight change in the slave laser power. As a result, the variations in amplitude of the generated waveform (dissimilar flatness) across the sub-intervals is observed. Fig. 5(a-iii) shows the frequency-time diagram of the SUDMC signal at the output of the PD, with a bandwidth of 4 GHz for both the up-chirp (12 GHz - 14 GHz) and the down-chirp (17.5 GHz - 15.5 GHz). Since only one beam is controlled with the AWG signal, the chirp rate in each sub-interval is the same for both the up- and down-chirp signals, which are 3 GHz/μs and 1 GHz/μs. The up-chirp signal is in the frequency ranges of 12 GHz - 13.5 GHz and 13.5 GHz - 14 GHz whereas the down-chirp signal is in the frequency ranges of 17.5 GHz – 16 GHz and 16 GHz - 15.5 GHz for the first and second sub-intervals. The generated down-chirp signal has a lower intensity than the up-chirp signal, as shown in Fig 5(a-iii). The low intensity may .e due to change in the power of the SL on injecting the ML1 and ML2 that suppress the power of SL slightly and also the power of ML2 is set to the minimum value to prevent SL shifting into injection locking state by suppressing the emission mode of SL.

To show the re-configurability of the generated SUDMC in terms of the number of chirps, bandwidth, and starting frequencies of the generated signal, a driving signal is modified

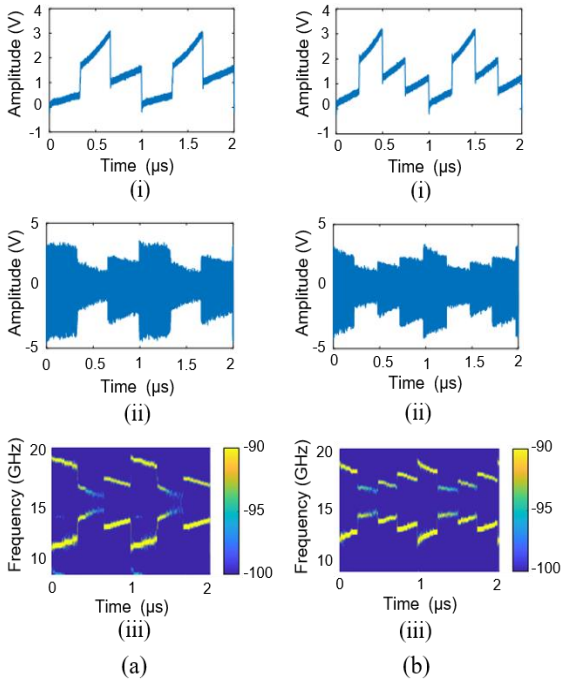

Fig. 6. SUDFHMC generation with (a) three chirps and (b) four chirps. (i) Amplitude-time AWG signal, (ii) instantaneous waveform of the generated signal, (iii) frequency-time diagram of the generated signal.

with three amplitude-time slopes, as shown in Fig. 5 (b-i). In this case, three sub-interval signals with equal intervals of 0.33 μs and voltage ranges of 0 V - 0.3 V, 0.3 V - 1.5 V, 1.5 V - 2.3

V are designed and applied to the MZM. Figure 5(b-ii) depicts the amplitude-time diagram of the generated signal. By changing the emission wavelengths of ML2 and ML1, the initial frequencies are changed, which can be seen in the frequency-time plot of Fig. 5 (a-iii and b-iii). The initial frequency is changed from 12 GHz (in a-iii) to 8 GHz (in b-iii) for up-chirp and 17.5 GHz (in a-iii) to 15 GHz (in b-iii) for down-chirp when comparing the two-chirp and three-chirp signals. The chirp-rates corresponding to the up-chirp signal are 3 GHz/μs (8 GHz - 9 GHz), 4 GHz/μs (9 GHz-10.3 GHz), and 3.6 GHz/μs (10.3 GHz - 11.5 GHz). Similarly, the chirp-rates corresponding to the down-chirp signal are 3 GHz/μs (15 GHz - 14 GHz), 4 GHz/μs (14 GHz - 12.7 GHz), and 3.6 GHz/μs (12.7 GHz – 11.5 GHz).

Like SUDMC, the SUDFHMC also uses two beam injection technique for the simultaneous generation of up- and down-chirp signals. In SUDFHMC, rather than the continuation of the frequency from one sub-interval to another, a sudden jump in the frequency is achieved. To generate the SUDFHMC waveform with three chirps and three frequency steps, a signal with three amplitude-time slopes is designed, as shown in Fig. 6 (a-i). As a result, starting frequency hopping, as well as change in the chirp-rate are achieved between the sub-intervals at the output of the O/E converter. However, the amplitude hopping between the subintervals is managed in such a way that the continuity of the signal is maintained by avoiding gaps and overlaps within the total interval of time. The designed amplitude-time slopes ensure that even though a hopping of start frequency is obtained in each sub-interval but no gaps and overlap on the total time interval. In this case also, the 1-μs time interval is divided into three equal sub-intervals with different voltage ranges of 0 V - 0.5 V and 1.6 V - 3 V, 1 V - 1.5 V, hence, three sub-intervals have different amplitude-time slopes which cause a different redshift rate in SL. The corresponding amplitude-time signal of the generated SUDFHMC signal is shown in Fig. 6 (a-ii). Fig. 6 (a-iii) shows the frequency-time diagram of the generated SUDFHMC with the up- and down-chirp signal with the start and stop frequencies of 10.5 GHz and 13 GHz; and 19 GHz and 16.5 GHz, respectively. The chirp rates for up-chirp signals are 3 GHz/μs, 3 GHz/μs, and 1.5 GHz/μs with the frequency range of 10.5 GHz - 11.5 GHz, 13 GHz - 14 GHz, and 12.5 GHz - 13 GHz, respectively. For down-chirp, signals of 3 GHz/μs, 3 GHz/μs, and 1.5 GHz/μs with the corresponding sub-interval frequency range of 19 GHz - 18 GHz, 16.5 GHz - 15.5 GHz, and 17 GHz - 16.5 GHz, respectively are observed.

To illustrate the flexibility in the generation of multi-step SUDFHMC, the control waveform is changed from three- to four-step hopping and with different amplitude-time slopes as shown in Fig. 6 (b-i) and applied to the MZM. As in the case of three-step hopping, the 1-μs interval is now divided into four equal sub-intervals of 0.25 μs with voltage ranges of 0 V - 0.75 V, 2 V - 3.1 V, 1.25 V - 1.9 V, and 0.75 V - 1.20 V. The amplitude-time signal of generated SUDFHMC is shown in Fig. 6(b-ii). Fig. 6(b-iii) shows the generated frequency-time signal of the SUDFHMC which has chirp-rates of 4 GHz/μs, 1.2 GHz/μs, 2.4 GHz/μs, and 2.8 GHz/μs for both the up- and down-chirp signal in their respective sub-intervals. The frequency range for up-chip signals in four sub-intervals is 11 GHz -12 GHz, 13.3 GHz -13.6 GHz, 12.7 GHz -13.3 GHz, and 12 GHz - 12.7 GHz. Whereas for the down-chirp, the sub-interval frequency ranges are 18.5 GHz - 17.5 GHz, 16.2 GHz - 15.9 GHz, 16.8 GHz - 16.2 GHz, and 17.5 GHz - 16.8 GHz.

V. Performance Analysis using Auto-Ambiguity Function

The normalized auto-ambiguity function is calculated to assess the delay-Doppler resolution of the generated CMC, SUDMC, and SUDFHMC signals. All the signals being evaluated have the same design specifications, which include a 1 μs time interval and a bandwidth of 7.0 GHz. Fig. 7(a) shows the plot of the auto-ambiguity function for a generated four-step SUDFHMC signal. Due to the presence of four sub-intervals (chirps) in a 1-μs interval, a considerable amount of sidelobes is observed, which can be filtered out with a low pass filter. However, a high degree of complexity in signal processing can arise while suppressing the undesired side-lobes if the signal has to be generated with a large number of chirps. Fig. 7(b) and 7(c) depict the zero Doppler cut and the zero delay cut values for four-step hoping with four chirps SUDFHMC signal. It is observed that the signal is compressed to 0.18 ns at -3 dB FWHM, leading to a high time-bandwidth product (TBWP) of 5555. Similarly, an unambiguous Doppler of 0.72 MHz is obtained at the zero-delay cut.

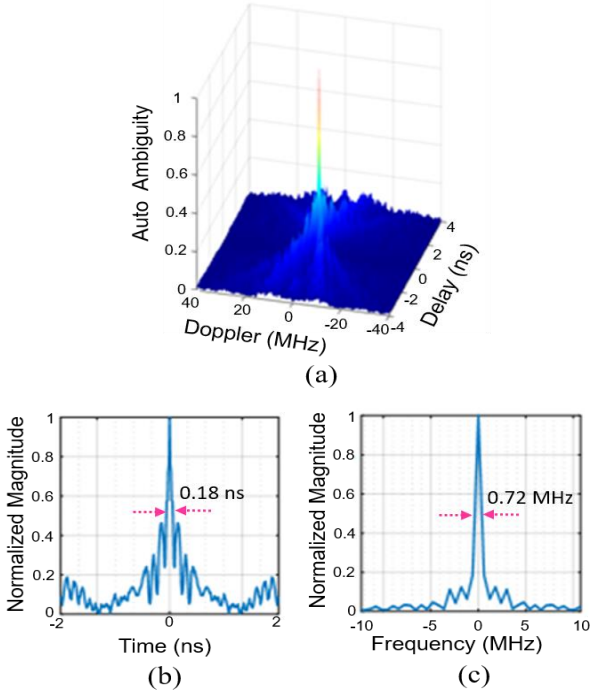

Fig. 7. Auto-ambiguity analysis of four step SUDFHMC. (a) Auto-ambiguity function, (b) and (c) ambiguity function at zero-Doppler cut, and zero delay cut.

A similar analysis was performed for the cases of two- and three-chirp CMC, SUDMC and SUDFHMC signals. In Fig. 8, the contour plots of the auto-ambiguity function of different signals at -3 dB FWHM are shown. As shown in Fig. 8, the FWHM delay of the three-chirp CMC is 0.22 ns, with two side lobes along with the main lobe, whereas the FWHM delays of three chirps SUDMC and SUDFHMC are 0.16 ns and 0.18 ns,

respectively, without the side lobes. This result indicates the simultaneous up-down chirp signals (SUDMC, SUDFHMC) offer superior compression characteristics and better side-lobes suppression than the continuous signal (CMC) for the identical signal design parameters.

Table (I) illustrates the obtained results of auto-ambiguity analysis for different types of signals. In the case of the CMC signal with three chirps, a delay of 0.22 ns, and a Doppler of 0.72 MHz at -3 dB FWHM are obtained, resulting in a TBWP of 4545. In the case of a three-chirp SUDMC signal, a delay of

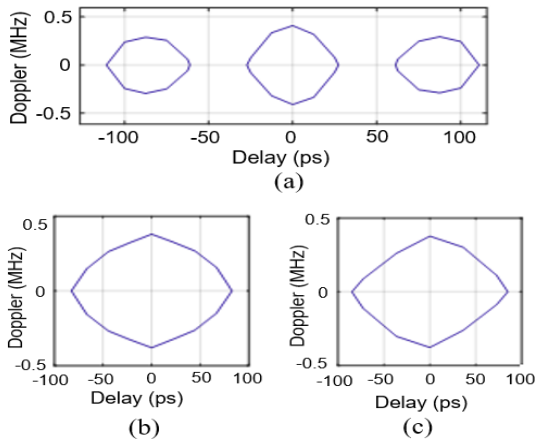

Fig. 8. Contour plots of auto-ambiguity function for (a) three-chirp CMC, (b) three-chirp SUDMC and c) three-steps, three-chirp SUDFHMC signals.

0.16 ns, a Doppler of 0.72 MHz at the -3 dB FWHM, and a TBWP of 6250 is observed. Moreover, as the number of sub-intervals increases within the given interval of the signal, the Doppler resolution has been slightly improved, as shown in Table 1. This improvement can be described as in the case of coherent pulse train waveform, as the number of pulses in the given signal interval increases, Doppler resolution improves [33].

TABLE I
SUMMARY OF AMBIGUITY ANALYSIS

Signal types	Delay @ FWHM of -3 dB (ns)	TBWP	Doppler @ FWHM of – 3 dB (MHz)
2-chirp CMC	0.22	4545	0.74
3-chirp CMC	0.22	4545	0.72
2-chirp SUDMC	0.16	6250	0.75
3-chirp SUDMC	0.16	6250	0.72
3-step, 3-chirp SUDFHMC	0.18	5555	0.75
4-step, 4-chirp SUDFHMC	0.18	5555	0.72

VI. CONCLUSION

In this paper, we presented a simple approach to generate multiple chirp-rate LFM waveforms photonically using one and two optical beam injection techniques. By designing the MZM drive signal with multiple amplitude-time slopes in a given interval, the rate of redshift in the SL is controlled. Thus, different chirp-rate signals can be generated within a time interval corresponding to each sub-interval redshift rate. In this work, the continuous multiple chirp (CMC) and simultaneous up-down multiple chirp (SUDMC, SUDFHMC) signals have been presented. On the comparative analysis of the output performance with identical design parameters (1-μs interval and 7.0 GHz bandwidth), the SUDMC and SUDFHMC outperformed the CMC signals in terms of range-Doppler resolution and side-lobes suppression. Ultra-fine, unambiguous delay and Doppler of 0.18 ns and 0.72 MHz, respectively, are achieved with the three-chirp, three-step hopping SUDFHMC, compared to 0.22 ns and 0.72 MHz for CMC with three chirps. Furthermore, the re-configurability in terms of bandwidth, center frequency, chirp-rate and the number of chirps are achieved by changing the wavelength spacing of the ML and SL, and the intensity control by the MZM drive signal. Due to the flexibility in generating and reconfiguring different waveform parameters, the proposed scheme can play an important role in multi-radar and multi-target applications for ultra-fine range-Doppler resolution and interference mitigation.

REFERENCES

[1] F. Scotti, F. Laghezza, P. Ghelfi and A. Bogoni, "Multi-Band Software-Defined Coherent Radar Based on a Single Photonic Transceiver," in *IEEE Transactions on Microwave Theory and Techniques*, vol. 63, no. 2, pp. 546-552, 2015, doi: 10.1109/TMTT.2014.2386877.

[2] Y. Tong, "Advanced Photonics-Based Radar Signal Generation Technology for Practical Radar Application," in *Journal of Lightwave Technology*, vol. 39, no. 11, pp. 3371-3382, 2021, doi: 10.1109/JLT.2021.3066588.

[3] W. Zou, H. Zhang, X. Long *et al*, "All-optical Central-frequency-Programmable and Bandwidth-tailorable Radar," in *Sci Rep*, vol. 6, no. 19786, 2016, doi: 10.1038/srep19786.

[4] A. Wang, D. Zheng, S. Du, J. Zhang, P. Du, Y. Zhu, W. Cong, X. Luo, Y. Wang, and Y. Dai, "Microwave Photonic Radar System with Ultra-flexible Frequency-domain Tunability," in *Opt. Express*, vol. 29, no. 9, pp. 13887-13898, 2021, doi:10.1364/OE.423952.

[5] S. Pan and Y. Zhang, "Microwave Photonic Radars," in *Journal of Lightwave Technology*, vol. 38, no. 19, pp. 5450-5484, 2020, doi: 10.1109/JLT.2020.2993166.

[6] Y. Zhang, C. Liu, Y. Zhang, K. Shao, C. Ma, L. Li, L. Sun, S. Li, and S. Pan, "Multi-Functional Radar Waveform Generation Based on Optical Frequency-Time Stitching Method," in *Journal of Lightwave Technology*, vol. 39, no. 2, pp. 458-464, 2021, doi: 10.1109/JLT.2020.3029275.

[7] P. Ghelfi, F. Laghezza, F. Scotti *et al*, "A Fully Photonics-based Coherent Radar System," in *Nature*, vol. 507, pp. 341–345, 2014, doi: 10.1038/nature13078.

[8] Zhang, F., Guo, Q. and Pan, S., "Photonics-based Real-time Ultra-high-range-resolution Radar with Broadband Signal Generation and Processing," in *Sci Rep.*, vol. 7, no. 13848, 2017, doi: 10.1038/s41598-017-14306-y.

[9] X. Li, S. Zhao, Z. Zhu, K. Qu, T. Lin and D. Hu, "Photonic Generation of Frequency and Bandwidth Multiplying Dual-Chirp Microwave Waveform," in *IEEE Photonics Journal*, vol. 9, no. 3, pp. 1-14, 2017, doi: 10.1109/JPHOT.2017.2705042.

[10] P. Zhou, F. Zhang, Q. Guo, S. Li and S. Pan, "Reconfigurable Radar Waveform Generation Based on an Optically Injected Semiconductor Laser," in *IEEE Journal of Selected Topics in Quantum Electronics*, vol. 23, no. 6, pp. 1-9, 2017, doi: 10.1109/JSTQE.2017.2699659.

[11] Fan-Yi Lin and Jia-Ming Liu, "Diverse Waveform Generation Using Semiconductor Lasers for Radar and Microwave Applications," in *IEEE*

Journal of Quantum Electronics, vol. 40, no. 6, pp. 682-689, 2004, doi: 10.1109/JQE.2004.828254.

[12] H. Chen, B. Nakarmi and S. Pan, "Multi-Band LFM Signal With Unidentical Bandwidths Subjected to Optical Injection in a DFB Laser," in *IEEE Photonics Technology Letters*, vol. 33, no. 8, pp. 391-394, 2021, doi: 10.1109/LPT.2021.3065387.

[13] B. Nakarmi, Y. Bai, C. Fang, X. Wang *et al*., "Photonically Generated Frequency Hopped Linear Frequency Modulated Signal Using a DFB Laser," in *Journal of Lightwave Technology*, vol. 40, no. 20, pp. 6729-6736, 2022, doi: 10.1109/JLT.2022.3174664.

[14] H. Chen, P. Zhou, L. Zhang, S. Bassi, B. Nakarmi and S. Pan, "Reconfigurable Identical and Complementary Chirp Dual-LFM Signal Generation Subjected to Dual-Beam Injection in a DFB Laser," in *Journal of Lightwave Technology*, vol. 38, no. 19, pp. 5500-5508, 2020, doi: 10.1109/JLT.2020.2993368.

[15] Y. Xu, T. Jin, H. Chi, S. Zheng, X. Jin and X. Zhang, "Photonic Generation of Dual-Chirp Waveforms With Improved Time-Bandwidth Product," in *IEEE Photonics Technology Letters*, vol. 29, no. 15, pp. 1253-1256, 2017, doi: 10.1109/LPT.2017.2712192.

[16] Y. Ding, S. Guo, H. Wu *et al*., "Dual-Chirp Photonics-Based Radar for Distance and Velocity Measurement Based on Compressive Sensing," in *IEEE Photonics Journal*, vol. 14, no. 4, pp. 1-7, 2022, doi: 10.1109/JPHOT.2022.3188846.

[17] S. Peng, S. Li, X. Xue, X. Xiao, D. Wu and X. Zheng, "A Photonics-Based Coherent Dual-Band Radar for Super-Resolution Range Profile," in *IEEE Photonics Journal*, vol. 11, no. 4, pp. 1-8, 2019, doi: 10.1109/JPHOT.2019.2929210.

[18] X. Zhu, G. Sun and F. Zhang, "Photonics-based Multiband Radar Fusion with Millimeter-level Range Resolution," *2022 Optical Fiber Communications Conference and Exhibition (OFC)*, San Diego, CA, USA, pp. 1-3, 2022, doi: 10.1364/OFC.2022.Th3G.2.

[19] K. Abratkiewicz, P. J. Samczyński, R. Rytel-Andrianik and Z. Gajo, "Multipath Interference Removal in Receivers of Linear Frequency Modulated Radar Pulses," in *IEEE Sensors Journal*, vol. 21, no. 17, pp. 19000-19012, 2021, doi: 10.1109/JSEN.2021.3087319.

[20] D.-H. Kim, H.-J. Kim, and J.-H. Lim, "Design of Optimized Coded LFM Waveform for Spectrum Shared Radar System," in *Sensors*, vol. 21, no. 17, pp. 5796, 2021, doi: 10.3390/s21175796.

[21] F. Uysal, "Phase-Coded FMCW Automotive Radar: System Design and Interference Mitigation," in *IEEE Transactions on Vehicular Technology*, vol. 69, no. 1, pp. 270-281, 2020, doi: 10.1109/TVT.2019.2953305.

[22] X. Yang, K. Zhang, T. Wang and Y. Zhao, "Anti-interference Waveform Design for Automotive Radar," *2017 IEEE 2nd Advanced Information Technology, Electronic and Automation Control Conference (IAEAC)*, Chongqing, China, pp. 14-17, 2017, doi: 10.1109/IAEAC.2017.8053967.

[23] M. Kronauge and H. Rohling, "New Chirp Sequence Radar Waveform," in *IEEE Transactions on Aerospace and Electronic Systems*, vol. 50, no. 4, pp. 2870-2877, 2014, doi: 10.1109/TAES.2014.120813.

[24] Y. Kitsukawa, M. Mitsumoto, H. Mizutani, N. Fukui and C. Miyazaki, "An Interference Suppression Method by Transmission Chirp Waveform with Random Repetition Interval in Fast-Chirp FMCW Radar," *2019 16th European Radar Conference (EuRAD)*, Paris, France, pp. 165-168, 2019.

[25] .F. Jin and S. Cao, "Automotive Radar Interference Mitigation Using Adaptive Noise Canceller," in *IEEE Transactions on Vehicular Technology*, vol. 68, no. 4, pp. 3747-3754, 2019, doi: 10.1109/TVT.2019.2901493.

[26] K. E. Kolodziej, J. G. McMichael and B. T. Perry, "Multitap RF Canceller for In-Band Full-Duplex Wireless Communications," in *IEEE Transactions on Wireless Communications*, vol. 15, no. 6, pp. 4321-4334, 2016, doi: 10.1109/TWC.2016.2539169.

[27] C. Ma, Y. Yang, F. Cao *et al*., "High-Resolution Microwave Photonic Radar with Sparse Stepped Frequency Chirp Signals," in *IEEE Transactions on Geoscience and Remote Sensing*, vol. 60, pp. 1-10, 2022, doi: 10.1109/TGRS.2022.3208112.

[28] P. Li, L. Yan, J. Ye *et al*., "Photonic-Assisted Leakage Cancellation for Wideband Frequency Modulation Continuous-Wave Radar Transceiver," in *Journal of Lightwave Technology*, vol. 38, no. 6, pp. 1178-1183, 2020, doi: 10.1109/JLT.2019.2954402.

[29] S. -K. Chan, S.-K. Hwang, and J.-M. Liu, "Period-one Oscillation for Photonic Microwave Transmission Using an Optically Injected Semiconductor Laser," in *Opt. Express*, vol. 15, no. 22, p. 14921, 2007, doi: 10.1364/oe.15.014921.

[30] X.-Q. Qi and J. M. Liu, Dynamics Scenarios of Dual-beam Optically Injected Semiconductor Lasers," in *IEEE Journal of Quantum Electronics*, vol. 47, no. 6, pp. 762–769, 2011, doi: 10.1109/JQE.2011.2115994.

[31] V. A. Thomas et al., "Millimeter-wave Radio Over Fiber Optical Upconversion Techniques Relying on Link Nonlinearity". *IEEE Communications Surveys & Tutorials*, vol. 18, no. 1, pp. 29-53, 2016. doi: 10.1109/COMST.2015.2409154.

[32] C. Tseng, Y. Hung, and S. Hwang, "Frequency-modulated Continuous-Wave Microwave Generation Using Stabilized Period-one Nonlinear Dynamics of Semiconductor Lasers," *Opt. Lett.*, vol. 44, no. 13, pp. 3334-3337, 2019, doi: 10.1364/OL.44.003334.

[33] N. Levanon, "Radar", in *Encyclopedia of Physical Science and Technology*, 3rd ed., Academic Press, 2003, pp. 497-510.

B. Nakarmi (S'11-M'17-SM'20) received B.E., M.E., and Ph.D. degrees in Electronics and communication, Information and communication engineering from Tribhuvan University, Nepal, Harbin engineering university, Harbin, China and Korea Advanced Institute of Science and Technology, Daejeon, Rep. of Korea in 2004, 2008, and 2012, respectively. He joined the College of Electronics and Information Engineering, Nanjing University of Aeronautics and Astronautics, China, in 2016, where he is currently a professor in the Key Laboratory of Radar Imaging and Microwave Photonics (Nanjing Univ. Aeronaut. Astronaut.), Ministry of Education. His research has focused on developing optical blocks used in optical communication and networks using Fabry-Pérot laser diode, bio-sensors based on nano-structures, and microwave photonics.

From 2012 to 2013, he worked as a Research and Development Manager in InLC technology Korea, Postdoctoral Researcher at Nanjing University (2012-2014), China. From 2014 to 2016, he was a Research Professor at KAIST. He has authored and co-authored over 100 research papers, including 40 peer-reviewed journals, 45 papers in conference proceedings and several invited papers and talks.

Prof. Nakarmi is a senior member of the Optical Society of America and IEEE. Prof. Nakarmi had served as a committee member in SPIE photonics ASIA 2012, IEEE ICECIT 2021, and a reviewer of several peer-reviewed journals.

Bai yan Song received a BS degree in electronic information engineering from the Nanjing University of Aeronautics and Astronautics, Jincheng college, China. Currently, he is a Master's student in electronics engineering at Nanjing University of Aeronautics and Astronautics, China.
His current research focuses on the areas of semiconductor laser diodes applications for microwave photonics.is a Master degree student in College of Electronics and Information Engineering at Nanjing University of Aeronautics and Astronautics, China. His current research focuses on the areas of semiconductor laser diodes applications for microwave photonics.

Ikechi Augustine Ukaegbu (M'12-SM'18) received his B.Sc. in Electrical Engineering, Electromechanics, and Electro-technology at Moscow Power Engineering Institute (Technical University), Moscow, Russia in 2004 and M.Sc. in Electronics and Microelectronics at the same university in 2006. He obtained his Ph.D. at the Korea Advanced Institute of Science and Technology (KAIST) in 2012. He has worked as a Postdoctoral researcher in Electrical Engineering Department at KAIST from 2012 to 2013. He held R&D positions at Electronics and Telecommunications Research Institute (ETRI), Korea, from 2008 to 2009 and at Lightron Fiber-Optics Inc., Korea in 2013. He also worked as a senior engineer with the design technology team at Samsung Electronics Co. Ltd, Korea, from 2013 to 2016. He co-founded a startup company where he served as the CTO from 2016 to 2017. He has been with Nazarbayev University School of Engineering since 2018 as an Assistant Professor in the Electrical and Computer Engineering Department. He is the director of Integrated Device Solutions and Nanophotonics Laboratory at Nazarbayev University, and his research interests include Circuits and Systems, Microwave & Nanophotonics, Signal & Power Integrity, Channel Modeling, and Sub-Terahertz Chip-to-chip links. More information can be found at www.idsnlab.info.

Hum Nath Parajuli (M'23) received an M. Eng. degree in Electronic and Information Engineering from Osaka University, Japan and M.Sc. degree in Photonic Networks Engineering from Scula Superiore Sant Anna, Italy and Ph.D. degree in Electrical Engineering from Budapest University of Technology and Economics, Hungary. He is currently a postdoctoral researcher in Nazarbayev University, Kazakhstan. His current research interests include photonics for radar and info-communication systems.

Aigerim Ashimbayeva (S'23) received her B.Eng. and M.Sc. degrees in Electrical and Electronic Engineering from Nazarbayev University School of Engineering in 2015 and 2017, respectively. Currently she is a doctoral student of Electrical Engineering program at the School of Engineering and Digital sciences, Nazarbayev University. She is currently with the Integrated Device Solutions and Nanophotonics Laboratory and her research interests include optoelectronics, microwave photonics, interference mitigation in RADARs and optical signals generation for photonic RADARs.

U. Nakarmi received BE in Electronics and Communication from Tribhuvan University, Nepal, in 2008. He received his MS and Ph.D. in Electrical Engineering from Oklahoma State University, OK, USA, and the State University of New York at Buffalo, NY, USA, in 2011 and 2018. From 2018 to 2020, Dr. Nakarmi was a Postdoctoral Fellow in the Department of Electrical Engineering and the Department of Radiology, Stanford University, CA, USA, before joining the Department of Computer Science and Computer Engineering at the University of Arkansas, AR, USA as an Assistant Professor.

Prof. Nakarmi's research interests span across areas of machine learning, big data, and signal processing with applications to computational imaging, radiology, and knowledge discovery from the data. His expertise lies in high dimensional data representation and reconstruction: encompassing techniques such as compressed sensing, sparse representation, nonlinear representation, and manifold learning.

Prof. Nakarmi is a member of IEEE and serves as a reviewer for several IEEE journals, including IEEE Transactions on Medical Imaging and IEEE Transactions on Computational Imaging. Dr. Nakarmi served as a PC member in IEEE International Conference on Big Data 2021, 2022.

Xiangchun Wang received a B.Eng. degree in automation and a Ph.D. degree in microelectronics and solid-state electronics from Nanjing University, Nanjing, China, in 2009 and 2015, respectively. He is currently an associate professor with the Key Laboratory of Radar Imaging and Microwave Photonics, Ministry of Education, Nanjing University of Aeronautics and Astronautics, Nanjing, China. His current research interests include microwave photonics measurement and optical fiber sensing technologies. He has authored and co-authored over 60 research papers, including over 32 peer-reviewed journals and 28 papers in conference proceedings.

Shilong Pan (S'06-M'09-SM'13-F'22) received the BS and Ph.D. degrees in electronics engineering from Tsinghua University, Beijing, China, in 2004 and 2008, respectively. From 2008 to 2010, he was a "Vision 2010" Postdoctoral Research Fellow in the Microwave Photonics Research Laboratory, University of Ottawa, Canada. He joined the College of Electronic and Information Engineering, Nanjing University of Aeronautics and Astronautics, China, in 2010, where he is currently a full professor and deputy director of the Key Laboratory of Radar Imaging and Microwave Photonics (Nanjing Univ. Aeronaut. Astronaut.), Ministry of Education.

His research has focused on microwave photonics, which includes optical generation and processing of microwave signals, ultrawideband over fiber, photonic microwave measurement, and integrated microwave photonics. Dr. Pan has authored or co-authored over 400 research papers, Including more than 250 papers in peer-reviewed journals and 150 papers in conference proceedings.

Prof. Pan is a Fellow member of the IEEE Microwave Theory and Techniques Society, the IEEE Photonics Society, the IEEE Instrumentation and Measurement Society, and a Fellow member of the Optical Society of America. He was selected to receive an OSA outstanding reviewer award in 2015. Dr. Pan is currently a Topical Editor for Chinese Optics Letters. He was a Chair of numerous international conferences and workshops, including the TPC Chair of IEEE ICOCN 2015, TPC Chair of the high-speed and broadband wireless technologies subcommittee of the IEEE Radio Wireless Symposium in 2013, 2014 and 2016, TPC Chair of the Optical fiber sensors and microwave photonics subcommittee chair of the OptoElectronics and Communication Conference in 2015, a Chair of the microwave photonics for broadband measurement workshop of International Microwave Symposium in 2015, a TPC Chair of the microwave photonics subcommittee of CLEO-PR, OECC and PGC 2017 (joint conference), and a TPC Co-Chair of IEEE MWP 2017.